INTERNATIONAL JOURNAL FOR NUMERICAL METHODS IN FLUIDS, VOL. 14, 1151–1171 (1992)

A NUMERICAL SIMULATION OF BOUNDARY LAYER EFFECTS IN A SHOCK TUBE

K. J. BADCOCK

Oxford University Computing Laboratory, 8–11 Keble Road, Oxford OX1 3QD, U.K.

SUMMARY

A numerical scheme is used to investigate boundary layer effects in a shock tube. The method consists of a mixture of Roe's approximate Riemann solver and central differences for the convective fluxes and central differences for the viscous fluxes and is implicit in one space dimension. Comparisons are made with experimental data and with solutions obtained via boundary layer equations. Examination of the calculated flow field explains the observed behaviour and highlights the approximate nature of boundary layer solutions.

KEY WORDS Shock tubes Boundary layers Roe's scheme Navier–Stokes

1. INTRODUCTION

Model experiments are used in the aerospace industry to investigate flow fields around aircraft. The required flow conditions can be generated by connecting a shock tube to a test section containing a model of the aircraft under consideration. Possible conditions range from subsonic to hypersonic, resulting in a wide variation in fluid velocities and temperatures. In addition, shock tubes can be used to study real gas effects such as deviations from ideal gas behaviour. A discussion of some applications can be found in Reference 1.

For any application it is necessary to know the flow conditions generated to enable interpretation of the results. If the flow is inviscid and the gas is assumed perfect, then the transient development is well understood (see e.g. Reference 1). In that case the flow can be modelled by the Euler equations in one dimension. However, there are a number of possible effects which can cause departures from the inviscid solution. These include viscosity and heat conduction and so-called real gas effects involving deviations from the ideal equations of state. In this paper we shall be concerned with the first two and shall neglect the last.

The departure from inviscid behaviour becomes especially marked when the shock tube is operating at low initial pressures (when the Reynolds number based on the tube radius and the peak velocity is typically about 500). This case is of particular interest for the investigation of high-altitude flow over re-entry vehicles. The experimental results of Reference 2 showed dramatic departures from the anticipated inviscid behaviour. One measure of shock tube performance which is of particular interest in experiments is the time interval for which the high-temperature conditions prevail. This time interval, called the test time, is given at some point in the tube by the time difference between the shock and the contact surface passing that point. Inviscid theory predicts that this time interval will increase linearly with distance from the diaphragm. It was reported in Reference 2 that for a fixed shock Mach number the test time

0271–2091/92/101151–21$10.50

Received May 1991
Revised October 1991

tended to a limiting value. It was also reported that the shock attenuation is highly non-linear. This behaviour was attributed to boundary layer effects.

Considerable effort in the 1950s and 1960s was devoted to evaluating boundary layer effects.[3] In Reference 4 the test time and the shock-to-contact-surface distance are related by an ordinary differential equation derived by considering a mass balance in the region between the shock and the contact surface. An estimate of the mass flow past the contact surface in the boundary layer is required. Boundary layer theory is used to give an expression for the boundary layer thickness δ at the contact surface, namely

$$\delta = \beta(Re)^{-1/2}, \tag{1}$$

where Re is the Reynolds number. The parameter β is estimated by various methods. In Reference 4 a value of $\beta = \sqrt{3}$ is suggested based on a correlation with experimental data. An analytical method of approximating β is also presented which involves a similarity solution of boundary layer equations in Crocco variables. An improved estimate of β is obtained in Reference 5 by taking into account the effect of the boundary layer on the free stream. This is done by finding a similarity solution of the uniform free stream problem and then adapting the solution by using the idea that the boundary layer at some point in a non-uniform free stream is the same as the boundary layer due to a uniform free stream with a different point of origin. It is concluded that the correlated value is reasonable except when the shock Mach number tends to unity. A different approach is used in Reference 6 to tackle the boundary layer–free stream interaction problem. The boundary layer equations are transformed so that the free stream boundary conditions are in a convenient format. The partial differential equations are then solved by expanding the solution in series form and numerically solving the resulting ordinary differential equations. Results obtained from this method are presented in References 5 and 7. In Reference 8 boundary layer equations in Crocco variables are solved for a uniform free stream for the entire flow between the expansion fan and the shock. The domain is divided into four regions and an appropriate similarity solution is given for each region.

We refer to these methods by the generic term 'boundary layer methods'. They provide a means of estimating viscous effects and correlate well with the available experimental data. However, several points arise. First, they are mainly concerned with the 'steady state' reached at the limiting test time. The experimental results of Reference 2 show that the problem is transient, with the steady state referred to lasting only over part of the tube. This transient behaviour casts doubt over some of the assumptions used in boundary layer methods. One example is the assumption of isentropic flow in the free stream between the shock and the contact surface. Secondly, the experimental results of Reference 2 suggest that the boundary layer thickens to be of the same order as the tube radius. This casts doubt on the applicability of boundary layer equations as a correct model and also suggests, in contrast to the assumption made in all the boundary layer methods mentioned above, that the flow in the inviscid region is two-dimensional. The present work aims to achieve several objectives:

(1) to examine the transient nature of the problem
(2) to give a full description of the flow field
(3) to examine the assumptions underlying boundary layer methods.

During the 1970s and the early 1980s a family of methods was developed for simulating one-dimensional inviscid flows with shocks. These are based on the method of Godunov[9] and they split the problem into a series of discrete Riemann problems (i.e. hyperbolic partial differential initial value problems with piecewise constant initial data). These problems are solved separately and their solutions are recombined to advance the flow to a later time. Popular

methods of solving the Riemann problem include the methods of Glimm,[10] Roe,[11] Harten[12] and Osher and Solomon.[13] These methods are first-order-accurate in time and space. To improve them to second-order accuracy without introducing spurious oscillations around discontinuities, a correction term is added which is limited by a function of the gradients of the flow.[14] The approximate Riemann solver–flux limiter approach gives a method of computing sharp and monotone shock wave profiles. These schemes are traditionally extended to two dimensions by operator splitting.[15–17] For viscous problems it has proved successful to calculate the inviscid terms in the simulation by one of the above methods, with central differencing being used for the remaining viscous terms. An implicit version of such a scheme is used in Reference 18 to compute aerofoil flows. This scheme uses linearizations in time of the flux functions given by Roe's scheme and the resulting linear system is solved using a sparse matrix solver. A similar method is used in Reference 19 to study shock wave–boundary layer interactions.

In this paper a simulation of the Navier–Stokes equations is used to examine low-pressure shock tube boundary layer effects. The numerical details are given. Then results are compared with the experiments of Reference 2 and the boundary layer solutions of Reference 5 to establish the performance of the method and to introduce the flow effects of interest. Finally, the flow field is considered to examine the behaviour of the previous section and some of the assumptions used to obtain the boundary layer solutions.

2. NUMERICAL METHOD

Consider the situation illustrated in Figure 1. The governing equations are assumed to be the thin layer Navier–Stokes equations which are written in the form

$$\frac{\partial \mathbf{w}}{\partial t}+\frac{\partial \mathbf{F}}{\partial x}+\frac{\partial \mathbf{G}}{\partial z}=\frac{\partial \mathbf{V}}{\partial z}, \tag{2}$$

where

$$\mathbf{w}=\begin{bmatrix}\rho\\ \rho u\\ \rho v\\ e\end{bmatrix}, \qquad \mathbf{F}=\begin{bmatrix}\rho u\\ \rho u^2+p\\ \rho uv\\ u(e+p)\end{bmatrix}, \qquad \mathbf{G}=\begin{bmatrix}\rho v\\ \rho uv\\ \rho v^2+p\\ v(e+p)\end{bmatrix},$$

$$\mathbf{V}=\begin{bmatrix}0\\ \mu\partial u/\partial z\\ (4\mu/3)\partial v/\partial z\\ u\mu\partial u/\partial z+v(4\mu/3)\partial v/\partial z+\kappa\partial T/\partial z\end{bmatrix}.$$

Here ρ, u, v, e, p, μ and κ denote the density, two components of velocity, energy, pressure, viscosity and heat conductivity respectively. The thermodynamic relations used to close the system are $p=(\gamma-1)\rho i$, where i is the specific internal energy defined by $i=e/\rho-(u^2+v^2)/2$, and $i=c_v T$. The constants γ and c_v represent the ratio of specific heats of the gas and the specific heat at constant volume respectively.

If we denote the boundary layer thickness by δ and the tube radius by R and if we assume[20] that $\partial/\partial x=O(1)$ and $\partial/\partial y=O(\delta/R)$, then an order-of-magnitude analysis shows that axial viscous terms may be neglected. From the radial momentum equation it follows that $\partial p/\partial y=O(\delta/R)$. In boundary layer theory this term is approximated by zero. However, we anticipate that $\delta/R=O(0{\cdot}1)-O(1)$ and hence we shall retain the fuller radial momentum equation with only the axial viscous term deleted.

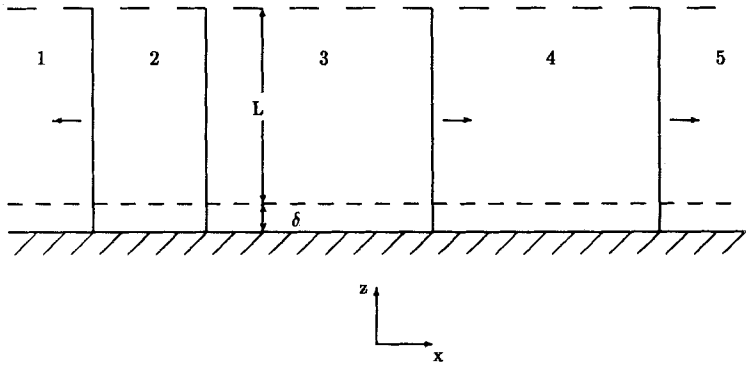

Figure 1. Flow structure in the shock tube. The numbers correspond to the regions labelled on the wave diagram (Figure 2), the upper dashed line denotes the centre of the tube, which is an axis of symmetry, and below the lower dashed line represents the region in which viscous effects are important

The discretization can be written in the form

$$\frac{\mathbf{w}_{i,j}^{n+1}-\mathbf{w}_{i,j}^{n}}{\Delta t}+\frac{\mathbf{F}_{i+1/2,j}^{n}-\mathbf{F}_{i-1/2,j}^{n}}{\Delta x}+\frac{\mathbf{G}_{i,j+1/2}^{n+1}-\mathbf{G}_{i,j-1/2}^{n+1}}{\Delta z}=\frac{\mathbf{V}_{i,j+1/2}^{n+1}-\mathbf{V}_{i,j-1/2}^{n+1}}{\Delta z}. \tag{3}$$

This represents a method which is implicit across the tube and explicit down the tube. The implicit part is used to allow boundary layers to be resolved without restricting the time step allowed by stability limits to impractical levels. The flux functions used are given by Roe's flux function with a superbee-limited correction[11, 14, 15, 21] for **F** and central difference flux functions for **G** and **V**, i.e.

$$\mathbf{G}_{i,j+1/2}=\tfrac{1}{2}(\mathbf{G}_{i,j}+\mathbf{G}_{i,j+1}). \tag{4}$$

V is constructed using the approximations

$$\frac{\partial v}{\partial z_{i,j+1/2}}=\frac{v_{i,j+1}-v_{i,j}}{\Delta z}, \tag{5}$$

$$v_{i,j+1/2}=\tfrac{1}{2}(v_{i,j}+v_{i,j+1}), \tag{6}$$

where v denotes u, v or T. The approximate Riemann solver–flux-limited correction approach is used to capture the shock and contact surface sharply and without spurious oscillations. The use of central differences is motivated by the need for linearizations in time of the flux functions **G** and **V** and also by the anticipated absence of discontinuities in the z-direction. The linearization

$$\Upsilon^{n+1}=\Upsilon^{n}+\sum_{j=1}^{M}\frac{\partial \Upsilon^{n}}{\partial \omega_j}(\omega_j^{n+1}-\omega_j^{n}) \tag{7}$$

is used as in Reference 22, where $\Upsilon=\Upsilon(\omega_1,\ldots,\omega_M)$ represents either **G** or **V**. This leads to a distinct tridiagonal system for each i at each time level and simplifies the computation. The choice of flux functions facilitates the calculation of the Jacobians required in the linearizations. The Jacobians for the viscous flux function are given in Appendix II. For the inviscid flux function the required expression is simply

$$\frac{\partial \mathbf{G}_{i,j+1/2}}{\partial \mathbf{w}_{i,k}}=\tfrac{1}{2}\mathbf{A}_{i,k} \tag{8}$$

where **A** is the well known Jacobian of **G** evaluated at the (i, k)th node.

The boundary conditions are imposed by extrapolating interior values and the boundary conditions onto fictitious nodes outside the computational domain. The usual algorithm is then applied to update all the interior nodes. A relation is required between the fictitious nodal values and the interior values to close the system of linear equations. Assume that the values at the fictitious node, denoted by a subscript 'f', depend only on the values at the node adjacent to the boundary, denoted by a subscript '*l*'. Then the functional dependence can be written

$$\mathbf{w}_f = \mathbf{g}(\mathbf{w}_l), \tag{9}$$

where **g** could be a non-linear function. Two types of boundary conditions will be considered, namely non-slip–imposed temperature conditions and non-slip–thermally insulated conditions. Common to the two is the requirement of no fluid flow at the boundary. Linear extrapolation from the interior node and the boundary conditions $u=0$ and $v=0$ gives

$$u_f = -u_l, \tag{10}$$

$$v_f = -v_l. \tag{11}$$

For no-heat-flow conditions at the boundary we assume, as in boundary layer theory, that the pressure is constant close to the boundary and we put $T_f = T_l$ to ensure that the temperature gradient at the boundary is zero as required by the thermally insulated condition. This leads to the expressions

$$\rho_f = \rho_l, \tag{12}$$

$$e_f = e_l. \tag{13}$$

Hence for the no-heat-flow case

$$\mathbf{g} = \begin{bmatrix} w_1 \\ -w_2 \\ -w_3 \\ w_4 \end{bmatrix} \tag{14}$$

and **g** is linear.

The situation when the boundary temperature is imposed is more complicated. In this case the pressure is again assumed constant close to the wall and so $p_f = p_l$. The internal energy i_w at the wall is known from the imposed temperature and the fictitious value is obtained from linear extrapolation to give $i_f = 2i_w - i_l$. Since the pressure, internal energy and velocity components are known, this allows **g** to be determined as

$$\mathbf{g} = \begin{bmatrix} hw_1 \\ -hw_2 \\ -hw_3 \\ w_4 + (h-1)K \end{bmatrix}, \tag{15}$$

where

$$K = \frac{w_2^2 + w_3^2}{2w_1}, \qquad h = \frac{i_l}{2i_w - i_l}. \tag{16}$$

For this case **g** is non-linear. To preserve the linearity of the equations, a linearization of **g** in time is performed to give

$$\mathbf{w}_f^{n+1} = \mathbf{g}_l^n + \boldsymbol{\Omega}(\mathbf{w}_l^{n+1} - \mathbf{w}_l^n), \tag{17}$$

where

$$\mathbf{\Omega}=\frac{\partial \mathbf{g}}{\partial \mathbf{w}}, \tag{18}$$

which is evaluated at $\mathbf{w}_1^n$. The expression for $\mathbf{\Omega}$ is given in Appendix II.

In practice, symmetry about the centre of the tube is exploited and one of the wall boundary conditions is replaced by the linear expression

$$\mathbf{g}=\begin{bmatrix} w_1 \\ -w_2 \\ w_3 \\ w_4 \end{bmatrix}. \tag{19}$$

The extension of the method to cylindrical geometries is given in Appendix I.

3. METHOD VERIFICATION

First, for the sake of reference, consider the inviscid solution. For given initial pressures and temperatures a shock and a contact surface propagate into the low-pressure gas with constant speeds and an expansion fan propagates into the high-pressure gas. The trajectories of these waves are shown in Figure 2. There is no attenuation and the test time, which increases linearly with distance, is given by

$$\tau=\left(\frac{1}{v_{cd}}-\frac{1}{v_s}\right)x, \tag{20}$$

where v_{cd} and v_s are the contact surface and shock speeds respectively and x is the distance from the membrane. The evolution depends on the pressure ratio and is independent of the actual pressure values. Some typical flows are given in Table I.

We now turn to the viscous problem. First a case is considered where $\delta/R \ll 1$. We anticipate that the solutions obtained by boundary layer methods will be accurate for this case. Boundary layer thicknesses computed from the present simulation are considered in Figure 3 for varying time steps and grid spacings across the boundary layer. The boundary layer thickness is defined in this paper as the distance from the boundary at which an axial velocity of 99% of the value at the

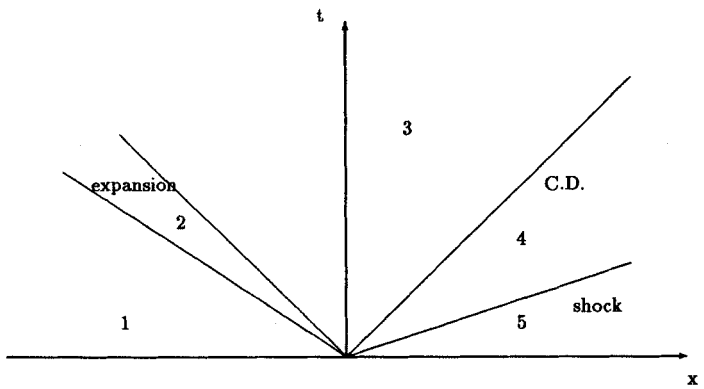

Figure 2. Wave trajectories for the inviscid solution

Table I. Shock tube flow parameters predicted by inviscid theory for ideal argon ($\gamma = 1{\cdot}66$). Here v_s and v_{cd} denoted the shock and contact surface velocities respectively. The shock Mach number is defined as v_s/c, where c is the sound speed ahead of the shock

Pressure ratio	Shock Mach number	v_s (m s^{-1})	v_{cd} (m s^{-1})	Rate of test time increase (μs m^{-1})
2	1·15	364	66	12385
4	1·31	416	132	5195
8	1·49	473	196	2983
11·9	1·60	507	233	2328
20	1·74	553	279	1773
40	1·94	615	340	1318
100	2·20	697	415	972
200	2·38	757	469	810

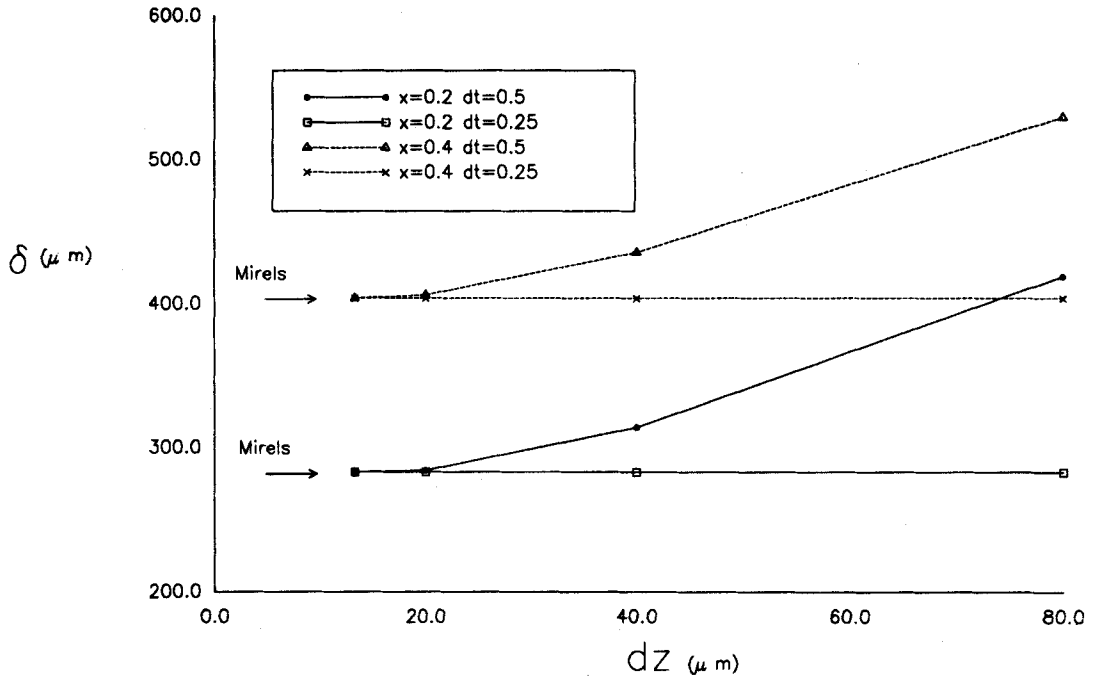

Figure 3. Boundary layer thickness δ computed from the present simulation as a function of radial grid spacing dz across the boundary layer at distances of 0·2 and 0·4 m from the shock and for time steps $dt = 0{\cdot}5 \times 10^{-5}$ and $2{\cdot}5 \times 10^{-5}$. These results are for a Mach 2 shock in air travelling into a pressure of 1 bar. The results from Reference 5 are $\delta = 283$ at 0·2 m and $\delta = 401$ at 0·4 m, values which are marked on the graph

centre of the tube is attained. The thicknesses are shown for distances of 0·2 and 0·4 m from the shock and the present values are compared with the values obtained by Mirels.[5] It is of interest to examine the convergence behaviour as the time step and the grid spacing are refined. From Figure 3 it can be seen that the boundary layer thicknesses do converge as the grid spacing is refined and that the limiting values are equal to the values from the boundary layer method of Reference 5. It is also clear that the effect of the limited time step refinement shown is consistent

with convergence as the time step is refined to the same limiting values obtained for the grid spacing refinement, although this convergence is not demonstrated on the figure.

The experimental results of Duff[2] show significant departures from the inviscid behaviour for flows in argon at low pressures. The shock was found to attenuate and the contact surface was found to accelerate. The shock attenuation is shown in Figure 4 and is non-linear. The two-dimensional Navier–Stokes solution shows similar behaviour but with an underlying numerical diffusion. To check that the numerical diffusion is not at a level which would invalidate the solutions, the problem's viscosity and heat conductivity were varied and the results are plotted in Figure 5. A parameter ε is defined as $\mu_p = \varepsilon\mu_{gas}$ and $\kappa_p = \varepsilon\kappa_{gas}$, where subscript 'p' denotes the value used in the simulation and subscript 'gas' denotes the gas value. The values of ε used in Figure 5 are $\varepsilon = \frac{1}{2}, \frac{1}{3}$ and 1, with these values being chosen because numerical diffusion should become more apparent as ε is reduced below unity. The boundary layer profiles thin and the shock wave attenuation decreases as the problem's viscosity is decreased, i.e. as ε is decreased. This suggests that numerical diffusion does not dominate the problem's viscosity.

It is well known from boundary layer theory that $\delta \propto (Re)^{-1/2}$, where Re is the Reynolds number. We shall assume that the changes in the reference density and velocity are small as ε is reduced. This is justified by the similarity of the boundary layer profiles obtained in Figure 5, which leads to a similarity of the flows in the inviscid core. Hence the value of $(\delta/\mu_p^{1/2})/\mu_{gas}^{1/2}$ should be independent of ε at a fixed distance from the shock if boundary layer theory is applicable. This value, denoted by Γ, is plotted as a function of the normalized distance between the shock and the contact surface in Figure 6. As can be seen, near the shock, which is located at a normalized distance of zero, where the boundary layer is relatively thin, all values of Γ for varying ε compare closely. However, closer to the contact surface, at a normalized distance of unity, the comparison becomes less close. It is expected that boundary layer theory will be more accurate as ε is

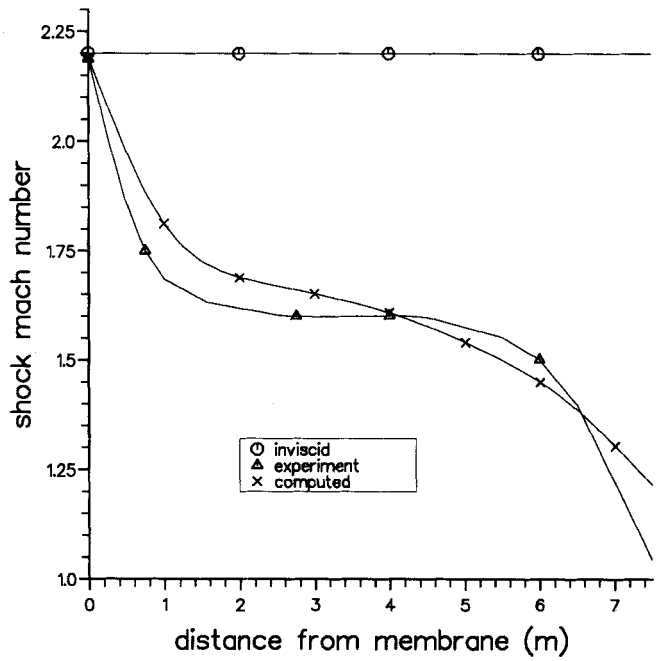

Figure 4. Shock mach number as a function of distance for an initial pressure of 67 Pa and a pressure ratio of 110. Inviscid theory gives a Mach number of 2·22. The experimental values are from Reference 2

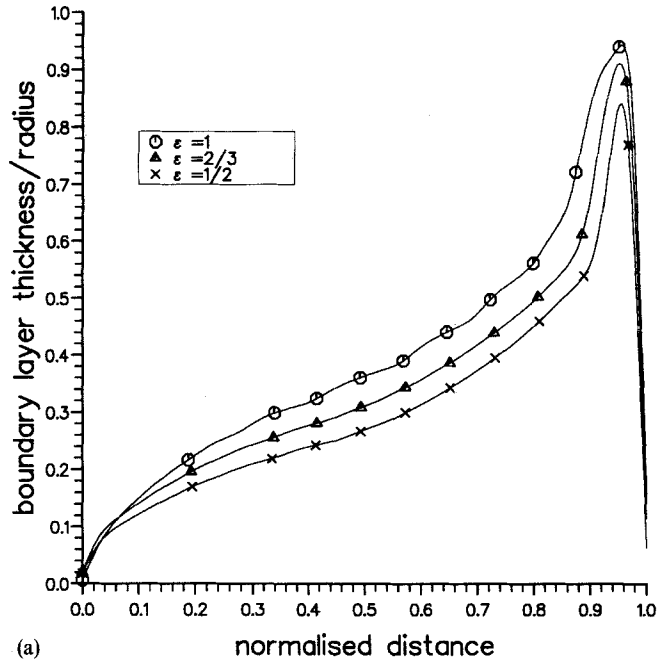

(a)

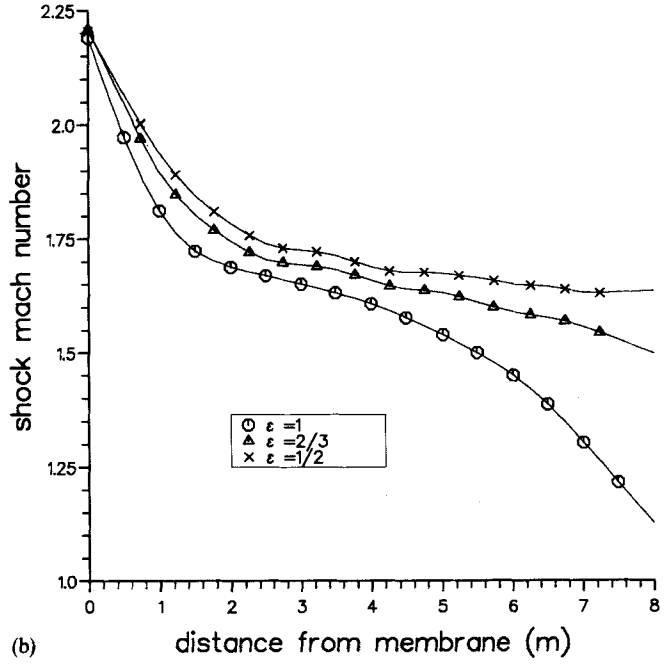

(b)

Figure 5. Shock Mach number and boundary layer thickness for various problem viscosities μ_p and heat conductivities κ_p, where $\mu_p = \varepsilon\mu_{gas}$, $\kappa_p = \varepsilon\kappa_{gas}$ and μ_{gas} and κ_{gas} are the gas values

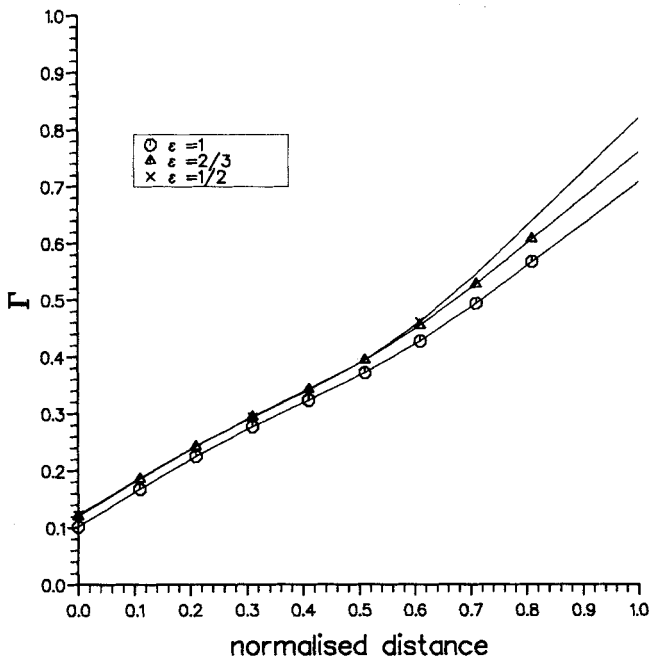

Figure 6. Γ plotted as a function of normalized distance from the shock to the contact surface for various values of the parameter ε. Here $\Gamma=(\delta/\mu_p^{1/2})/\mu_{gas}^{1/2}$

decreased because the boundary layers obtained become thinner. Hence we are particularly interested in the comparison between Γ for the physical values of μ and κ corresponding to $\varepsilon=1$ and the smaller values of ε. Note the almost exact match in the profiles of Γ between the cases $\varepsilon=\frac{1}{2}$, and $\varepsilon=\frac{2}{3}$, suggesting that boundary layer theory is appropriate for these cases, whereas there is some divergence between $\varepsilon=1$ and these two cases. This suggests that boundary layer theory is breaking down as a model for the cases which are examined in Reference 2.

Further evidence of the non-linear attenuation of the shock is found by examining the pressure ratio required to produce a shock of a specified strength as a function of distance. This function is plotted for a Mach 1·6 shock in Figure 7. Again the present results show reasonable agreement with experiment and a non-linear behaviour is observed.

The behaviour of the test times is particularly striking when compared to the inviscid behaviour. As noted above, inviscid theory predicts a test time increasing linearly with distance from the membrane. It was found experimentally that the test time actually tended to a limiting value. The test times found by the present method are given in Table II along with those predicted by the boundary layer method of Reference 23 and the experimental[2] and inviscid values. As can be seen, the present values are in reasonable agreement with the experimental and boundary layer values and it is clear that inviscid theory is useless for these cases. It is surprising that the values obtained by the boundary layer approach are quite so good for the lower-Mach-number shocks, since the boundary layers involved become of a comparable width to the tube radius. Hence the approximation involved in assuming no radial pressure gradient, as discussed in Section 2, must be considered questionable.

In conclusion, the numerical simulation of the two-dimensional Navier–Stokes equations shows qualitative and respectable quantitative agreement with experiment and it is reasonable to

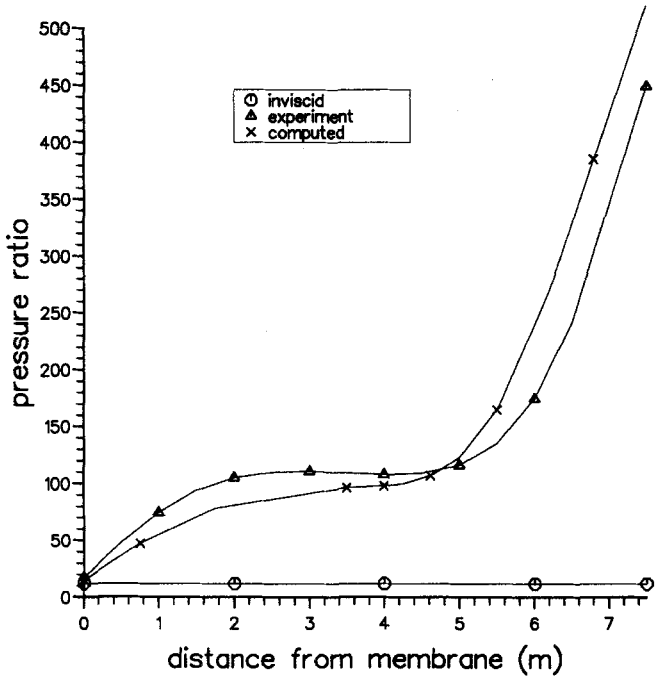

Figure 7. Pressure ratio required to produce a shock Mach number of 1·6 as a function of distance for an initial pressure of 67 Pa. Inviscid theory gives a constant ratio of 11·9. The experimental values are from Reference 2

Table II. Test times (in microseconds) for a variety of shock Mach numbers at a distance of 2·5 m from the membrane for a pressure ahead of the shock of 67 Pa. The boundary layer results are those of Mirels[23] and the experimental values are those of Duff[2]

Shock Mach number	Present results	Mirels	Experiment	Inviscid
1·4	670	418	330	9593
1·6	360	311	250	5925
1·8	230	253	160	4070
2·0	160	202	150	3090

use the solutions obtained to examine the flow effects more carefully. This is done in the next section.

4. CONSIDERATION OF THE FLOW FIELD

The wave trajectories for the inviscid and viscous solutions are plotted in Figure 8. The attenuation of the shock and the acceleration of the contact surface are evident. The two main points of interest are the non-linear attenuation of the shock and the question as to why the contact surface accelerates.

To consider these questions, the boundary layer thickness was plotted as a function of the normalized distance between the shock and the contact surface at several fixed times. The profiles are shown in Figure 9. The peak thickness is achieved at the contact surface as in Reference 8.

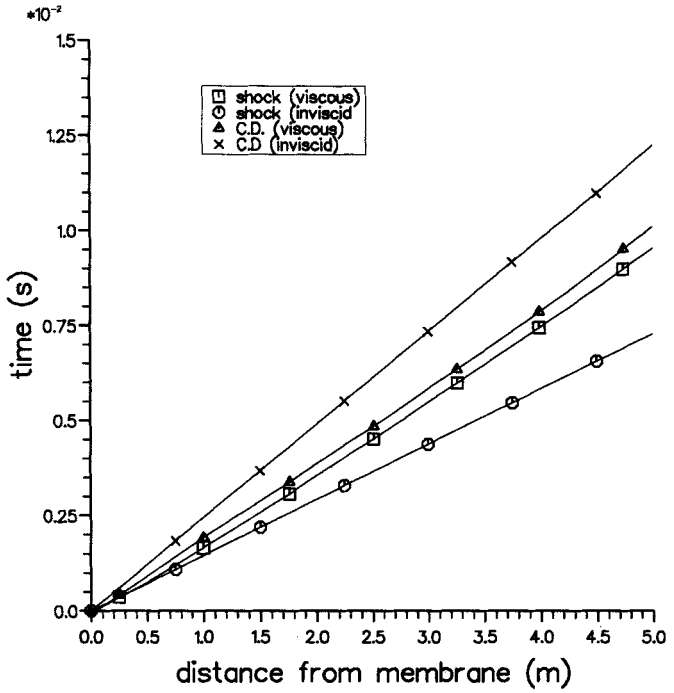

Figure 8. Wave trajectories for a pressure ratio of 100 and an initial pressure of 66·7 Pa

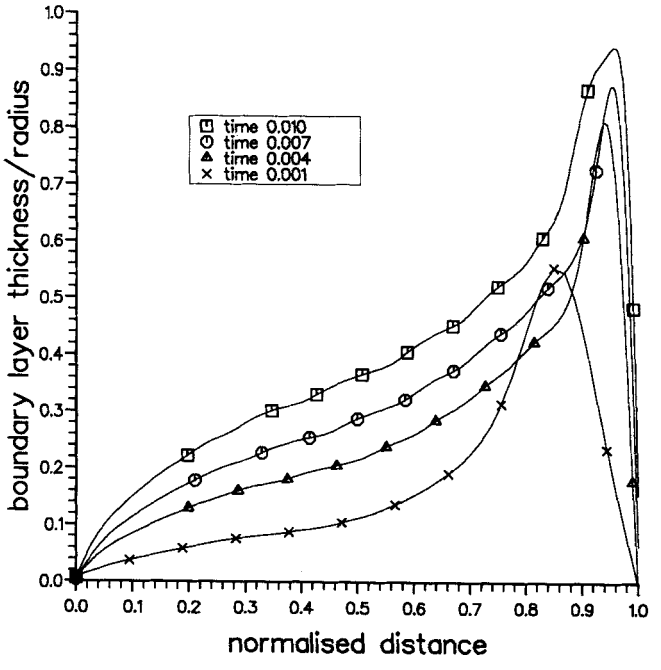

Figure 9. Boundary layer profiles for an initial pressure ratio of 100 and a pressure of 66·67 Pa ahead of the shock

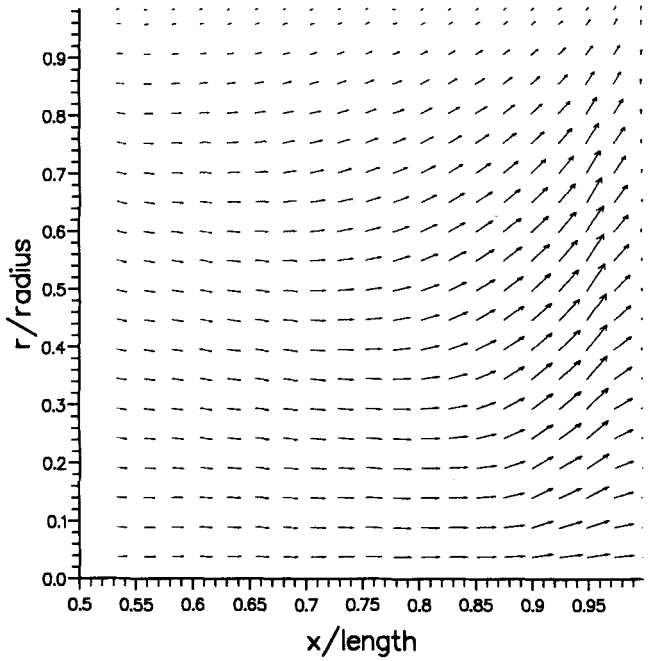

Figure 10. Velocity vectors for an initial pressure ratio of 100 and a pressure of 66·67 Pa ahead of the shock at time 0·1 s (Note the different length scaling in the axial and radial directions.)

If we consider the flow as being divided into two parts, the viscous region and the inviscid region, an analogy can be drawn between the flow in the inviscid region and the flow through a converging–diverging nozzle. The plot of the velocity field in Figure 10 shows the fluid in the inviscid region flowing in a manner consistent with the nozzle analogy. In the case of the nozzle the flow accelerates through the throat of the nozzle where the fluid is compressed. The plot of the flow parameters down the centre of the shock tube given in Figure 11 is consistent with this behaviour. The axial velocity increases up to the contact surface and then decreases thereafter. In addition, the flow is more compressed at the contact surface than is the case in the inviscid shock tube solution. This behaviour explains the acceleration of the contact surface, which moves with the fluid velocity. Notice the slight oscillation in density near the shock. This appears to be a numerical artefact and could be caused by the initial approximate projection onto the eigenvectors required in Roe's scheme.

The non-linear attenuation of the shock can also be examined. Initially, the rapid attenuation of the shock can be ascribed to the nozzle-type effect altering the parameters at the shock. Once this initial rapid change has settled down, the shock velocity remains constant over a length of the shock tube. During this time the boundary layer is growing slowly. In Figure 12 the velocity and temperature on the axis of the tube at the upstream side of the shock and at the contact surface are plotted. It can be seen that the velocity at the contact surface starts to attenuate at around 2 m from the membrane, with the rate of attenuation speeding up with distance. Further, the velocity at the upstream side of the shock behaves correspondingly. Following the nozzle analogy, a lower 'inlet' velocity at the contact surface to the diverging part of the nozzle leads to a lower 'outlet' velocity at the shock. An examination of the boundary layer thickness shows that the attenuation at the contact surface is due to viscous attenuation. Similarly, the thermal boundary layer starts

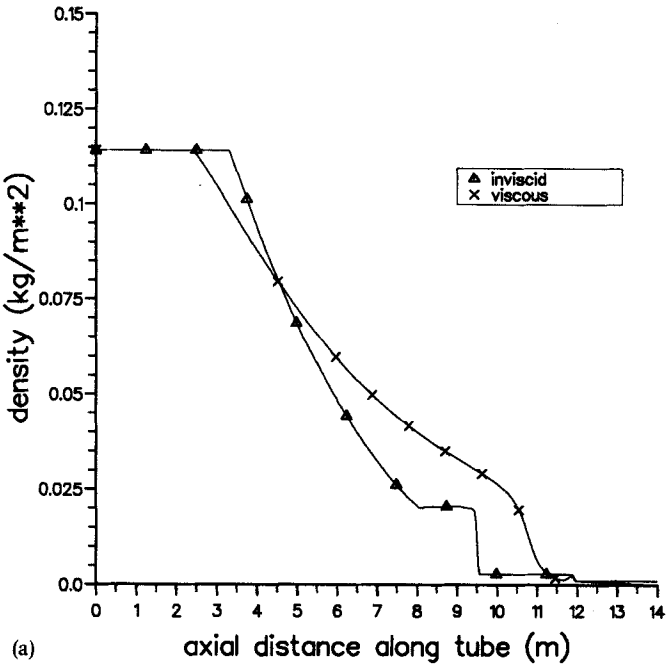

(a)

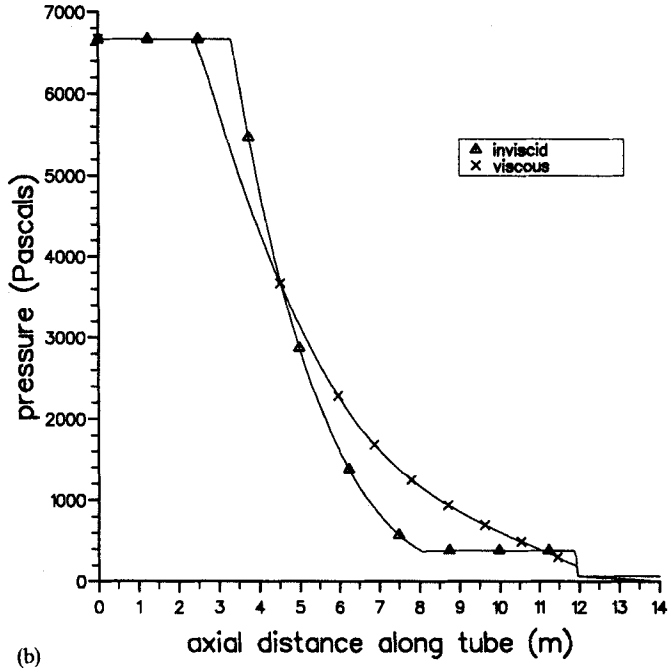

(b)

Figure 11. Solutions down the centre of the tube at time 0·1 s for an initial pressure ratio of 100 and a pressure of 66·67 Pa ahead of the shock

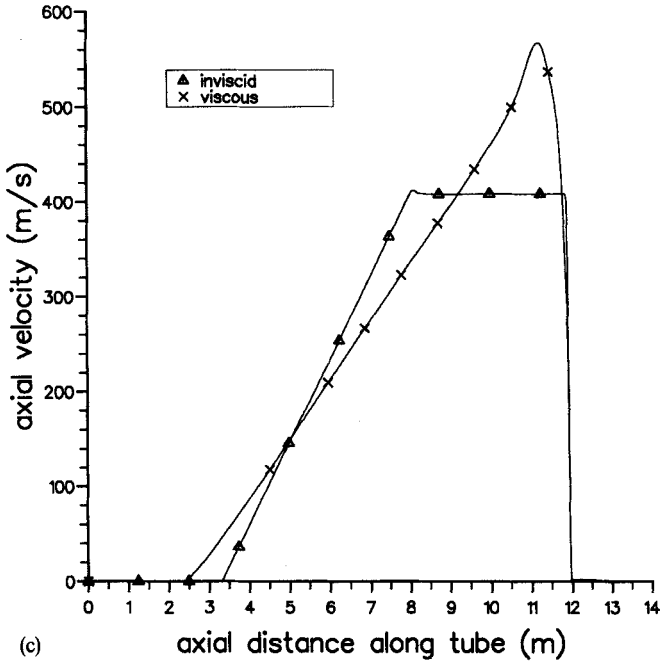

(c)

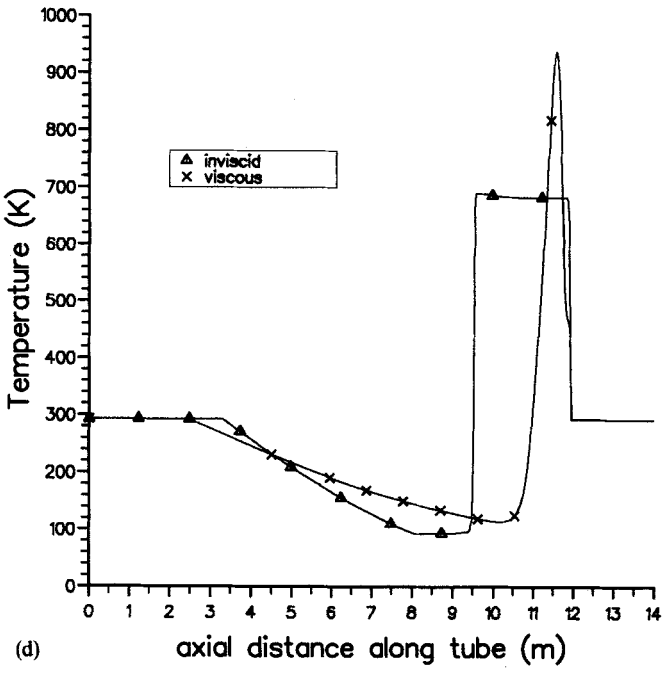

(d)

Figure 11. (Continued)

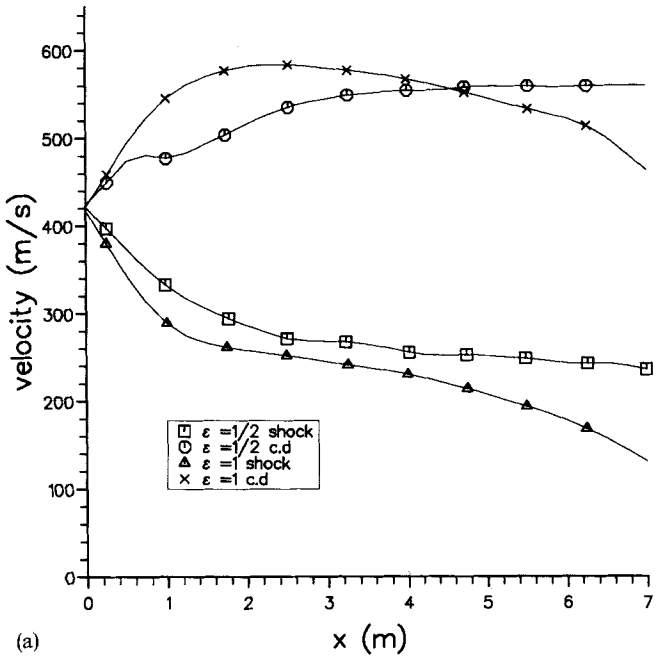

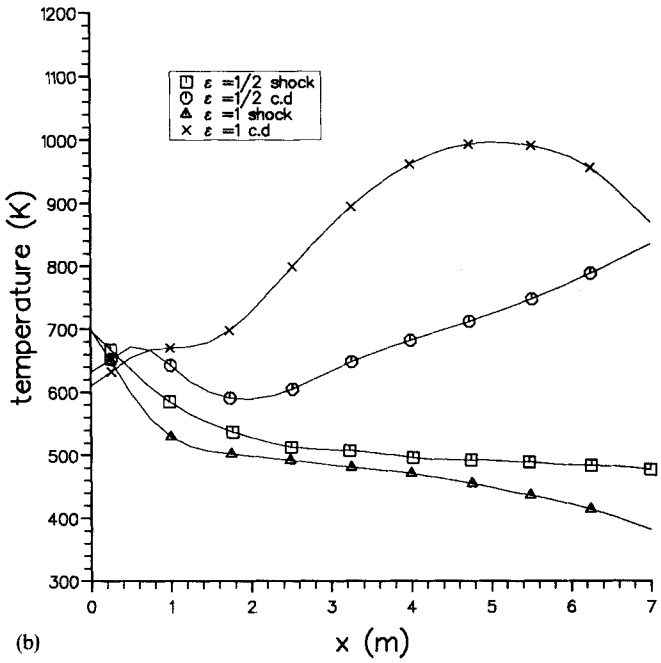

Figure 12. Values of the flow parameters along the tube axis at the shock and the contact surface

to take effect at the contact surface at around 5 m from the membrane, with a corresponding cooling at the shock. Hence it is surmised that the second region of attenuation of the shock observed by Duff[2] is due to the growth of the boundary layers at the contact surface to fill the tube, thus affecting the flow in the 'inviscid region', a term which is now used only for consistency with the above descriptions of the flow. Both the fluid velocity attenuation and the thermal cooling due to the boundary layer effects act to decrease the shock velocity, since the density tends to increase with decreasing temperature, and the shock velocity is given by the Rankine–Hugoniot condition

$$v_s = \frac{u_u}{1-\rho_d/\rho_u}, \tag{21}$$

where the subscript 'u' denotes conditions upstream of the shock and the subscript 'd' denotes conditions downstream of the shock. This expression decreases both with decreasing u_u and with increasing ρ_u. To test this scenario, the values for $\varepsilon = \frac{1}{2}$ are also plotted in Figure 12. It was noted above (see Figure 6) that the second stage of the shock attenuation was absent for this case. It can be seen that the boundary layer effects at the contact surface are also absent, lending support to the explanation given.

We shall now consider some of the assumptions required to obtain results via the boundary layer equations in the light of the current solutions. First, it should be noted that some of the boundary layers examined in this paper grow at the contact surface to fill the tube. As mentioned above, this begs the question as to how applicable the boundary layer equations are for these cases. The results for cases in which the boundary layers remain thin agree closely with the boundary layer results of Reference 5. Secondly, all the boundary layer solutions require the assumption that the shock speed is constant and that the flow is uniform in the shock's frame of reference. It is evident from Duff's experiments and from the present computations that this is only true on a finite interval and is certainly not true in the region near the membrane. This transient behaviour is not considered in the boundary layer methods. It is also assumed that the flow between the shock and the contact surface is isentropic. This is consistent with neglecting the shock attenuation. The entropies computed by the present method show an increase from the shock to the contact surface by about a factor of three. The solution of Reference 5 takes into account the non-uniformity of the flow between the shock and the contact surface, although still retaining the isentropic assumption.

Ratios of values at the contact surface to those at the shock are shown in Table III. There are several factors which might contribute to the discrepancies between the present values and the values obtained from Reference 5. It was noted above that the fluid at the contact surface is subject to viscous dissipation at around 2 m from the membrane where the shock Mach number is 1·69. The entropy and temperature at the contact surface both rise. This effect accounts for

Table III. Ratios of values at the contact surface to values immediately behind the shock. The results of Mirels[5] are included for comparison

Method	Mirels		Present results		
Shock Mach number	1	2	1·79	1·62	1·44
Temperature	1·33	1·12	1·26	2·02	2·32
Density	1·54	1·19	0·98	0·71	0·77
Pressure	2·05	1·33	1·23	1·43	1·79
Entropy	1·0	1·0	1·27	2·52	2·76

some of the differences between the two sets of results. It also should be noted that δ/R is of order 0·1–1, which calls into question the validity of boundary layer equations as a model for this situation and also the one-dimensional assumption of the velocity boundary condition at the boundary layer edge.

In Reference 8 the solution upstream of the contact surface is calculated but a uniform free stream is assumed. The boundary layer profiles computed from the two-dimensional Navier–Stokes simulation agree qualitatively with those obtained there. In particular, the increase in thickening just upstream of the contact surface and at the end of the expansion are noted.

5. CONCLUSIONS

The use of a simulation of the two-dimensional unsteady Navier–Stokes equations to investigate boundary layer effects in shock tubes allows a more detailed examination of the flow field with fewer simplifying assumptions than required for the boundary layer equation methods. In the method used in this paper the flow is assumed to be governed by the thin layer Navier–Stokes equations. This is justified by the type of solution expected and obtained, i.e. the flows remain convection-dominated in the axial direction with viscous effects being important in the radial direction along with small but significant radial convection. The thermodynamics of the gases is assumed to be adequately described by the perfect gas law. This is questionable because of the high temperatures encountered. However, it should be noted that this is not an assumption required by the solution method (see e.g. Reference 21). The code used in this study could be modified to account for real gas effects provided that the relevant experimental data describing the thermodynamics are available. The one-dimensional implicit formulation gives significant improvements in execution time. It was found that the one-dimensional implicit version of the code ran about half as quickly as the explicit version. However, the allowable time step increases by several orders of magnitude (by three orders of magnitude for the conditions of Figure 3). This makes it practical for the code to be run on workstations.

The flow fields from the simulation suggest that boundary layer development can cause the flow in the inviscid core to behave like the flow through a converging–diverging nozzle. This analogy helps to explain the observed phenomena involving the arrival times of the shock and the contact surface. The results also suggest that the flow in the region assumed to be inviscid is eventually subject to viscous dissipation, accounting for the non-linear attenuation of the shock.

The advantage of the present method over a boundary layer approach is that it does not have to

(1) focus only on the flow between the contact surface and the shock
(2) assume steady flow
(3) neglect shock attenuation
(4) assume a one-dimensional velocity boundary condition at the boundary layer edge
(5) assume isentropic flow between the shock and the contact surface.

Some or all of these simplifications are required by all boundary layer equation methods. However, it should be noted that the present method can be far more expensive computationally, since the boundary layer approach of Reference 6, for example, requires the solution of ordinary differential equations as opposed to partial differential equations. Our comparisons with experimental results show that the boundary layer methods give reasonable results, especially when the shock Mach number is not close to unity. The present method is more convincing than boundary layer methods for cases where the shock Mach number is close to unity and is more flexible with

respect to thermal boundary conditions and the specification of gas properties such as viscosity and thermodynamic properties.

Finally, with experimental data and asymptotic approximations available, the low-pressure shock tube problem is useful as a test problem for algorithms which solve the two-dimensional transient, compressible Navier–Stokes equations.

ACKNOWLEDGEMENTS

The author would like to acknowledge the help of Dr. I. J. Sobey in the preparation of this work. He would also like to thank the Science and Engineering Research Council for financial support. This work forms part of the research programme of the Oxford–Reading Institute for Computational Fluid Dynamics.

APPENDIX I: CYLINDRICAL EXTENSIONS

The extension of the scheme to cylindrical co-ordinates is not difficult. Using the same notation as in the rectangular case and denoting the radial distance by r and the axial distance by x, the Navier–Stokes equations become

$$\frac{\partial \mathbf{w}}{\partial t}+\frac{\partial \mathbf{F}}{\partial x}+\frac{1}{r}\frac{\partial (r\mathbf{G})}{\partial r}=\frac{1}{r}\frac{\partial (r\mathbf{V})}{\partial r}+\mathbf{C}, \tag{22}$$

where the additional term $\mathbf{C}$ is given by

$$\mathbf{C}=\begin{bmatrix} 0 \\ 0 \\ -p/r-(2u/3r)(\partial\mu/\partial r+2\mu/r) \\ (1/r)\partial(-2\mu u^2/3)/\partial r \end{bmatrix} \tag{23}$$

The discretization follows along similar lines to the rectangular case with the following notes. For the linearizations in time we note that, by the chain rule,

$$\nabla\mu=c_v\frac{\partial\mu}{\partial T}\nabla i, \tag{24}$$

where $\partial\mu/\partial T$ is known and ∇i is given above. Also, a straightforward calculation gives, for an ideal gas,

$$\nabla p=(\gamma-1)(\mathbf{E}-\nabla K), \tag{25}$$

where the ith component of $\mathbf{E}$ is given by δ_{i4}, with δ_{ij} denoting the (ij)th component of the Kronecker delta.

APPENDIX II: JACOBIANS FOR THE LINEARIZATIONS

To construct a system of linear equations, the Jacobians of the flux functions and the boundary conditions are required. In this appendix these Jacobians are derived.

For convenience consider the kinetic energy function K and the specific internal energy i given by

$$K=\frac{1}{2}\left(\frac{w_2^2}{w_1}+\frac{w_3^2}{w_1}\right), \tag{26}$$

$$i=\frac{w_4-K}{w_1}. \tag{27}$$

The vector of unknowns $\mathbf{w}=(w_1, w_2, w_3, w_4)^T$ here represents the conserved variables $(\rho, \rho u, \rho v, e)^T$. The gradients of these functions are then given by

$$\nabla K=\begin{bmatrix} -K/w_1 \\ w_2/w_1 \\ w_3/w_1 \\ 0 \end{bmatrix}, \tag{28}$$

$$\nabla i=\begin{bmatrix} -(\partial K/\partial w_1+i)/w_1 \\ -w_2/w_1^2 \\ -w_3/w_1^2 \\ 1/w_1 \end{bmatrix}. \tag{29}$$

The gradient of the function h defined in equation (16) is given by

$$\frac{\partial h}{\partial w_k}=\frac{2h^2 i_w}{i_1^2}\frac{\partial i}{\partial w_k}, \tag{30}$$

where $\partial i/\partial w_k$ is given by (29). The expressions for $\mathbf{\Omega}$ in (18) are given by

$$\Omega_{1,k}=\delta_{1,k}h+w_1\frac{\partial h}{\partial w_k}, \qquad \Omega_{2,k}=-\delta_{2,k}h-w_2\frac{\partial h}{\partial w_k},$$

$$\Omega_{3,k}=-\delta_{3,k}-w_3\frac{\partial h}{\partial w_k}, \qquad \Omega_{4,k}=\delta_{4,k}+K\frac{\partial h}{\partial w_k}+(h-1)\frac{\partial K}{\partial w_k}, \tag{31}$$

where δ_{ik} denotes the Kronecker delta and $1\leqslant k\leqslant 4$.

Now consider the Jacobians of the viscous flux function $\mathbf{V}_{i,j+1/2}$ given by the central difference approximations resulting from the approximations (5) and (6). We shall consider the Jacobian with respect to $\mathbf{w}_{i,j+1}$, since the one with respect to $\mathbf{w}_{i,j}$ follows similarly. First define the constants

$$\zeta_1=-\frac{2}{3(\Delta z)_{j+1/2}}(\mu_{i,j}+\mu_{i,j+1}), \qquad \zeta_2=\tfrac{3}{4}\zeta_1, \qquad \zeta_3=\frac{\kappa_{i,j}+\kappa_{i,j+1}}{-2c_v(\Delta z)_{j+1/2}} \tag{32}$$

Writing the velocity components as $u=w_2/w_1$ and $v=w_3/w_1$, it follows immediately that $\nabla u=(-w_2/w_1^2, 1/w_1, 0, 0)^T$ and $\nabla v=(-w_3/w_1^2, 0, 1/w_1, 0)^T$. We can then evaluate the required Jacobian J as

$$J_{1,k}=0, \qquad J_{2,k}=\zeta_2\frac{\partial u}{\partial w_k}, \qquad J_{3,k}=\zeta_1\frac{\partial v}{\partial w_k}, \tag{33}$$

$$J_{4,k}=u_{i,j+1/2}J_{2,k}+v_{i,j+1/2}J_{3,k}+\frac{1}{2}\zeta_2\frac{\partial u}{\partial w_k}+\frac{1}{2}\zeta_1\frac{\partial v}{\partial w_k}+\zeta_3\frac{\partial i}{\partial w_k},$$

where $1\leqslant k\leqslant 4$.

REFERENCES

1. A. Ferri, *Fundamental Data Obtained from Shock-tube Experiments*, Pergamon, Oxford, 1961.
2. R. E. Duff, 'Shock-tube performance at low initial pressure', *Phys. Fluids*, **2**, 207–216 (1959).

3. V. P. Korobeinikov, *Unsteady Interaction of Shock and Detonation Waves in Gases*, Hemisphere, New York, 1989.
4. A. Roshko, 'On flow duration in low-pressure shock tubes', *Phys. Fluids*, **3**, 835–842 (1960).
5. H. Mirels, 'Correlation formulas for laminar shock-tube boundary layer', *Phys. Fluids*, **9**, 1265–1272 (1966).
6. H. Mirels and W. S. King, 'Series solutions for shock-tube laminar boundary layer and test time', *AIAA J.*, **4**, 782–789 (1966).
7. H. Mirels, 'Flow nonuniformity in shock tubes operating at maximum test times', *Phys. Fluids*, **9**, 1907–1912 (1966).
8. J. D. A. Walker and S. C. R. Dennis, 'The boundary layer in a shock tube', *J. Fluid Mech.*, **56**, 19–47 (1972).
9. S. K. Godunov, 'A finite difference method for the numerical computation of discontinuous solutions of the equations of fluid dynamics', *Math. Sb.*, **47**, 271–306 (1959).
10. J. Glimm, 'Solutions in the large for nonlinear hyperbolic systems of equations', *Commun. Pure Appl. Math.*, **18**, 697–715 (1965).
11. P. L. Roe, 'Approximate Riemann solvers, parameter vectors and difference schemes', *J. Comput. Phys.*, **43**, 357–372 (1981).
12. A. Harten, 'High resolution schemes for hyperbolic conservation laws', *J. Comput. Phys.*, **49**, 357–393 (1983).
13. S. Osher and F. Solomon, 'Upwind difference schemes for hyperbolic conservation laws', *Math. Comput.*, **38**, 339–374 (1982).
14. P. K. Sweby, 'High resolution schemes using flux limiters for hyperbolic conservation laws', *SIAM J. Numer. Anal.*, **21**, 995–1011 (1984).
15. P. L. Roe, 'Characteristic-based schemes for the Euler equations', *Ann. Rev. Fluid Mech.*, **18**, 337–365 (1986).
16. G. Moretti, 'Computations of flows with shocks', *Ann. Rev. Fluid Mech.*, **19**, 313–337 (1987).
17. C. H. Cooke and K. S. Fansler, 'Comparison with experiment for TVD calculations of blast waves from a shock tube', *Int. j. numer. methods fluids*, **9**, 9–22 (1989).
18. V. Venkatakrishnan, 'Viscous computations using a direct solver', *Comput. Fluids*, **18**, 191–204 (1990).
19. M. S. Liou, 'A Newton/upwind method and numerical study of shock wave/boundary layer interactions', *Int. j. numer. methods fluids*, **9**, 747–761 (1989).
20. C. A. J. Fletcher, *Computational Techniques for Fluid Dynamics, Vol. 2*, Springer-Verlag, Berlin, 1988.
21. P. Glaister, 'An approximate Riemann solver for the three-dimensional Euler equations with a general equation of state using operator splitting', *Numerical Analysis Rep. 11*, Department of Mathematics, Reading University, 1986.
22. V. Venkatakrishnan, 'Newton solution of inviscid and viscous problems', *AIAA J.*, **27**, 885–891 (1989).
23. H. Mirels, 'Test time in low-pressure shock tubes', *Phys. Fluids*, **6**, 1201–1214 (1963).